Electrochimica Acta 55 (2010) 3714–3720

Contents lists available at ScienceDirect

Electrochimica Acta

journal homepage: www.elsevier.com/locate/electacta

Formation of Cu/Pd bimetallic crystals by electrochemical deposition

A.E. Alvarez, D.R. Salinas *,[1]

Instituto de Ingeniería Electroquímica y Corrosión (INIEC), Departamento de Ingeniería Química, Universidad Nacional del Sur, Avda. Alem 1253, 8000 Bahía Blanca, Argentina

ARTICLE INFO

Article history:
Received 7 September 2009
Received in revised form
21 December 2009
Accepted 20 January 2010
Available online 28 January 2010

Keywords:
Electrodeposition
Palladium
Cu/Pd
Bimetallic crystals
AFM

ABSTRACT

The early stages of the palladium electrodeposition process onto a vitreous carbon (VC) substrate as well as the deposition of Cu on such Pd/VC modified surface were investigated using classical electrochemical techniques, atomic force microscopy (AFM) and scanning electron microscopy (SEM). Within the potential range considered the kinetics of the Pd electrodeposition from a $PdCl_2$ acid solution can be described by a model involving progressive nucleation on active sites and diffusion-controlled 3D growth. The nucleation rate constant, A_0, and the number of active sites of the substrate, N_0, were determined from the analysis of potentiostatic current transients on the basis of an existing theoretical model. The AFM images corroborated the progressive nucleation mechanism showing irregular palladium crystals randomly distributed over the VC surface, with different sizes and 3D morphological characteristics. The electrodeposition of Cu was carried out onto the characterized Pd/VC modified surface from a Cu^{2+} containing solution using a well defined polarization routine. The SEM/EDX images confirmed the formation of Cu/Pd bimetallic crystals uniformly distributed on the VC surface and the in situ AFM images obtained during this process corroborated that Cu formed a core–shell structure with the Pd crystals. Nevertheless, the subsequent anodic stripping produced only a partial dissolution of the Cu deposits, and therefore, the formation of a Cu/Pd alloy could be inferred.

1. Introduction

The formation of catalytically active metal particles on chemically inert electrode surfaces is important not only for fundamental surface science but also for the preparative aspect of nanotechnology. Electrochemical techniques are considered to be well-suited tools for the formation of such micro- or nanostructures since supersaturation and undersaturation can be well adjusted and also rapidly changed via the electrode potential. Usually, practical noble metal electrodes are prepared with a small amount of these metals highly dispersed on a conductive low-cost solid substrate. This practice provides a large surface area on which many reactions were reported to proceed at accelerated rates [1]. Since the activity of the noble metal deposits strongly depends on the surface structure, studies on the growth mechanism and the structural characterization on an atomic level are essential to develop a better understanding in this field. Therefore, the study of the first stages of these electrochemical phase formation processes is a topic of central importance as they seem to be significant in determining the morphology and physicochemical properties of the electrodeposited particles [2].

The modification of solid surfaces by palladium micro- or nanocrystals is a special case due to its recognized high catalytic activity [3,4]. Different studies on electrodeposition of palladium microparticles have been developed but information on the very initial eletrodeposition stages is limited [5–8]. In addition, the system Cu/Pd has been demonstrated as effective electrocatalyst for different electrochemical reduction reactions, specially, for the cathodic reduction of nitrate [9–13]. Considering this information, in the present work the early stages of the palladium electrodeposition onto a vitreous carbon (VC) substrate from a $PdCl_2$ acid solution were investigated using classical electrochemical techniques and atomic force microscopy (AFM) and scanning electron microscopy (SEM). VC was chosen as foreign substrate because carbonaceous materials are the preferred supports for Pd electrocatalysts due to their high overpotential for hydrogen evolution and their properties as inert and low-cost materials. Additionally, the formation of Cu/Pd bimetallic particles obtained by electrodeposition of Cu onto the Pd/VC modified surface was also analysed. The formation of bimetallic particles by electrochemical deposition can be considered as an interesting alternative method for the preparation and subsequent basic characterization of catalysts such those used in fuel cells [14,15]. Therefore, the preparation methodology

* Corresponding author. Tel.: +54 291 4595182; fax: +54 291 4595182.
E-mail address: dsalinas@uns.edu.ar (D.R. Salinas).
[1] ISE member.

0013-4686/$ – see front matter © 2010 Elsevier Ltd. All rights reserved.
doi:10.1016/j.electacta.2010.01.076

used in this work can be extended to other bimetallic systems with technological interest.

2. Experimental details

Palladium particles were electrodeposited onto a VC electrode from a 9.5×10^{-4} M $PdCl_2$ + 0.1 M Na_2SO_4 + 2.4×10^{-2} M HCl solution (pH 2.6) prepared from supra-pure chemicals (E. Merck, Darmstadt) and fourfold quartz-distilled water. The electrodeposition of Cu^{2+} onto a palladium modified VC surface (Pd/VC) was produced from a 1×10^{-3} M $CuSO_4$ + 0.1 M Na_2SO_4 solution. In the last case the solution pH was adjusted to 2.6 with the addition of H_2SO_4. The electrolytes were deaerated by bubbling highly purified nitrogen prior to each experiment.

The electrochemical measurements were carried out at a temperature T = 298 K in a conventional three-electrode electrochemical cell. The working electrode was a VC rod sealed into a Teflon holder, with an exposed area of 0.070 cm^2. The electrode surface was mechanically polished with progressively finer diamond paste up to 1 μm until a mirror-like finished surface was obtained. Then, it was washed with fourfold quartz-distilled water. A saturated calomel electrode (SCE) mounted inside a Luggin capillary and a platinum sheet (1 cm^2) were used as reference and counter electrode, respectively. All potentials in this paper were referred to SCE.

The cyclic voltammetric measurements and the chronoamperometric studies were carried out employing a computer controlled potentiostat-galvanostat EG&G Princeton Applied Research Model 273A. Cyclic voltammograms were carried out at a sweep rate $|dE/dt| = 10\ mV\ s^{-1}$.

The initial stages of Pd deposition on VC or Cu onto the Pd/VC modified surface were studied using a standard Nanoscope III AFM microscope (Digitals Instruments, Santa Barbara, USA) operated in the contact mode. A scanner of 15 μm, and oxide-sharpened silicon nitride probes (Veeco Probes) with a nominal tip-radius between 5 and 40 nm and spring constant of 0.06 N m^{-1} were used. Scanning electron microscopy (SEM) studies were carried out using a JEOL 35CF microscope, with an accelerating voltage of 15 keV, integrated with an energy dispersive X-ray system (EDX) EDAX DX-4.

3. Results and discussion

3.1. Electrodeposition of Pd particles

3.1.1. Voltammetric response

Cyclic voltammetry was utilised to evaluate the palladium electrodeposition on VC in a qualitative form. Voltammetric polarization curves were obtained in the potential range $-350\ mV \le E \le 900\ mV$ and the scans were initiated at 850 mV. The voltammetric response (Fig. 1) is typical of a nucleation and growth process and there was no evidence of adsorption peaks in the underpotential (*upd*) range, even at an increased sensitivity of the current scale, which indicates a weak deposit–substrate interaction [2]. During the first scan towards the negative direction the main feature observed is the cathodic current peak at $E \approx 150$ mV which is associated to the Pd deposition on VC. Other cathodic current peaks are observed in the potential range $-250\ mV \le E \le -150\ mV$ which are characteristic of the hydrogen atoms adsorption onto the Pd particles [16,17] previous to the onset of H_2 evolution recorded at $E \approx -300$ mV.

On the reverse scan and after the anodic peaks related to the hydrogen oxidation and desorption processes, an anodic current density peak is observed at $E \approx 520$ mV, related to the Pd particles oxidation. A current crossover is recorded and the corresponding crossover potential, $E_{co} \approx 400$ mV, is independent of the negative

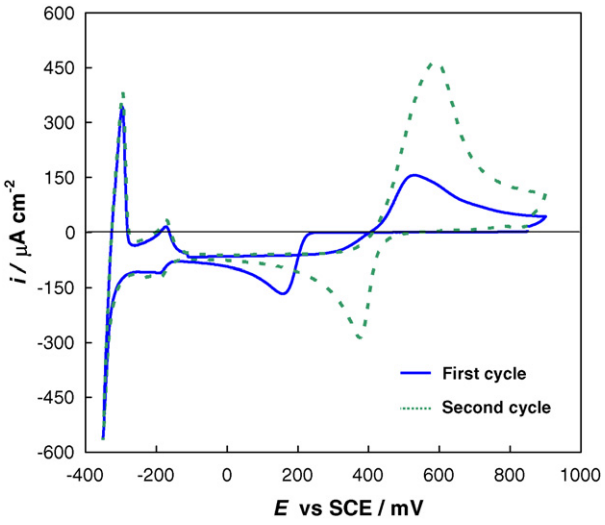

Fig. 1. Cyclic voltammograms for the system VC/9.5×10^{-4} M $PdCl_2$ + 0.1 M Na_2SO_4 + 2.4×10^{-2} M HCl (pH 2.6), T = 298 K, $|dE/dt| = 10\ mV\ s^{-1}$.

reverse potential, indicating that under the experimental conditions of this voltammetric study the electrodeposition process was controlled by charge transfer. According to Fletcher et al. [18] under this type of control the E_{co} value should correspond to the equilibrium potential of the metal redox couple. The residual anodic current observed at the anodic limit suggests the passivation of these particles. Therefore, a residual metal deposit is present on the VC at the end of the voltammetric cycle. During the second voltammetric cycle the deposition initiates at $E \approx 430$ mV which corroborates the presence of a residual metal deposit on the VC surface. These residual particles act as active sites requiring lower energy for the subsequent discharge of the metallic ions. Table 1 shows the different soluble palladium species that would be involved in the electrodeposition process [6]; the corresponding stability constants, K [19]; the calculated equilibrium concentrations, C; the standard electrode potentials at 298 K, E^0 [20]; and the calculated equilibrium potentials for the related electrochemical reactions, E_{eq}. Therefore, the experimental potential value $E \approx 430$ mV is in agreement with the thermodynamic values shown in Table 1 and also with the experimental E_{co} value. In addition, the thermodynamic data indicate that in the potential range $374\ mV \le E \le 430\ mV$ the reduction of $PdCl_4^{2-}$ is favoured, while for $E < 373$ mV all soluble Pd(II) species can be reduced.

3.1.2. Chronoamperometric analysis

The nucleation process of Pd onto VC from the Pd(II) containing solution was analysed using the potential step technique. Fig. 2 shows a family of potentiostatic current transients obtained from E_{start} = 700 mV to different overpotentials, η_{Pd}, defining $\eta_{Pd} = E - 430$ mV, and considering that at E = 430 mV initiates the electrochemical reduction of Pd(II) species according to the previous discussion. The transients exhibit the typical shape for a nucleation process with three-dimensional growth of nuclei limited by diffusion of the electroactive species [21]. After an initial current peak, related to the double-layer charging, the current increases due to the formation and growth of discrete nuclei. At later stages of the nucleation process the individual diffusion zones of adjacent nuclei overlap, and the current reaches a maximum and then decays following the usual $t^{-1/2}$ dependence according to the Cottrell equation. The 3D-nucleation model with hemispherical diffusion control to the growing 3D clusters describes the kinetics of electrolytic phase formation at the early stages, when diffusion of the depositing species from the bulk of the solution

Table 1
Electrodeposition of Pd on VC substrate from a 9.5×10^{-4} M $PdCl_2$ + 0.1 M Na_2SO_4 + 2.4×10^{-2} M HCl solution. Thermodynamic data.

Species	Reaction	Log K	E^0 vs. SCE (mV)	C (M)	E_q vs. SCE (mV)
Cl^-				2.29×10^{-2}	
Pd^{2+}	$Pd^{2+} + 2e \leftrightarrows Pd^0$		710	3.10×10^{-9}	458
$PdCl^+$	$PdCl^+ + 2e \leftrightarrows Pd^0 + Cl^-$	4.47	529	2.09×10^{-6}	409
$PdCl_2$	$PdCl_2 + 2e \leftrightarrows Pd^0 + 2Cl^-$	7.74	396	8.91×10^{-5}	373
$PdCl_3^-$	$PdCl_3^- + 2e \leftrightarrows Pd^0 + 3Cl^-$	10.20	325	5.88×10^{-4}	374
$PdCl_4^{2-}$	$PdCl_4^{2-} + 2e \leftrightarrows Pd^0 + 4Cl^-$	11.50	350	2.68×10^{-4}	430

to the electrode/solution interface is the slow step of the process, considering the eventual overlap of diffusion zones and the development of nucleation exclusion zones around already established nuclei. Depending on the substrate/electrolyte system, the nucleation involves two limiting cases. In the extreme case of *instantaneous nucleation*, all nuclei are immediately formed after it is applied a potentiostatic step. On the other hand, for *progressive nucleation*, the number of nuclei increases gradually with the deposition time. Different theoretical models of nucleation [21–26], recently reviewed [27], have been developed and tested over the last 20 years in order to predict the behaviour of the potentiostatic current transients. Sharifker and Hills [21] have proposed a convenient method to identify the nucleation mechanism. The method is based on rendering the curves dimensionless by referencing the current density, i, to the maximum current density, i_m, and the time, t, to the time corresponding to the maximum current density, t_m. The following equations result for instantaneous (Eq. (1)) and progressive (Eq. (2)) nucleation:

$$\left(\frac{i}{i_m}\right)^2 = 1.9542\left\{1 - \exp\left[-1.2564\left(\frac{t}{t_m}\right)\right]\right\}^2\left(\frac{t}{t_m}\right)^{-1} \quad (1)$$

$$\left(\frac{i}{i_m}\right)^2 = 1.2254\left\{1 - \exp\left[-2.3367\left(\frac{t}{t_m}\right)^2\right]\right\}^2\left(\frac{t}{t_m}\right)^{-1} \quad (2)$$

Therefore, the experimental data may be presented in a non-dimensional plot, $(i/i_m)^2$ vs. t/t_m, in order to be compared with the theoretical transients obtained from Eqs. (1) and (2). Fig. 3 shows a non-dimensional plot of the experimental current transients at different overpotentials, for the electrodeposition of Pd on VC. In this case, the palladium nucleation follows the response predicted for 3D-progressive nucleation controlled by diffusion of electroactive species.

In order to extract quantitative information on the kinetic parameters associated with the crystal nucleation and growth process, the model proposed by Heerman and Tarallo [26] was applied. According to this model, which merges the approaches of Sharifker–Mostany [22] and Sluyter-Rehbach et al. [23], the nucleation rate constant per site, A, and the number density of active sites over the substrate surface, N_0, can be obtained by fitting the entire experimental current transients to the following expression:

$$i(t) = zFDc\frac{1}{(\pi Dt)^{1/2}}\frac{\Phi}{\Theta}\{1 - \exp[-\alpha N_0(\pi Dt)^{1/2}t^{1/2}\Theta]\} \quad (3)$$

where

$$\Phi = 1 - \frac{\exp(-At)}{(At)^{1/2}}\int_0^{(At)^{1/2}} \exp(\lambda^2)d\lambda \quad (4)$$

$$\Theta = 1 - \frac{(1 - e^{-At})}{At} \quad (5)$$

with $\alpha = 2\pi(2MDc/\rho)^{1/2}$, zF: molar charge transferred during electrodeposition, c: metal ion bulk concentration, M: molar mass of the deposit, D: diffusion coefficient. The function Φ is directly related to the Dawson's integral and reflects the retardation of the current by slow nucleation, and Θ reflects the retardation of the growth of the coverage as a result of slow nucleation. Fig. 4 shows, as examples, a comparison between the experimental transients obtained at three overpotentials and the corresponding theoretical transients obtained by fitting the Eq. (4) to the experimental data using A, N_0 and D as fitting parameters. As it is shown, the Heerman and Tarallo theory could be applied with sufficient accuracy in the potential range studied and the best-fit of these variables are listed in Table 2. From the results obtained it is possible to conclude that N_0 increased as the potential was changed to more negative values. This behaviour indicates the existence of a site energies distribu-

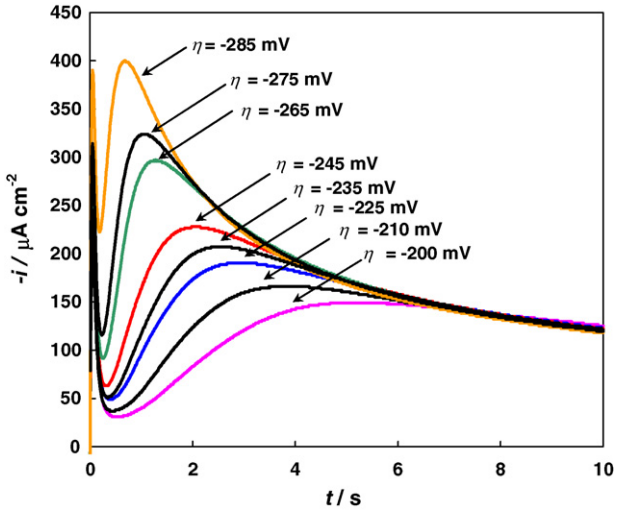

Fig. 2. Typical family of potentiostatic current transients for the nucleation of Pd on VC at different overpotentials, η, from solution 9.5×10^{-4} M $PdCl_2$ + 0.1 M Na_2SO_4 + 2.4×10^{-2} M HCl (pH 2.6).

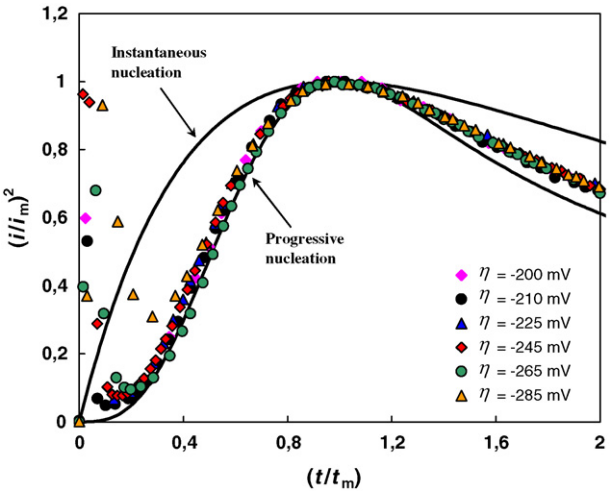

Fig. 3. Comparison of theoretical non-dimensional plots for instantaneous nucleation from Eq. (1) and progressive nucleation from Eq. (2), to the experimental current transients of Fig. 2.

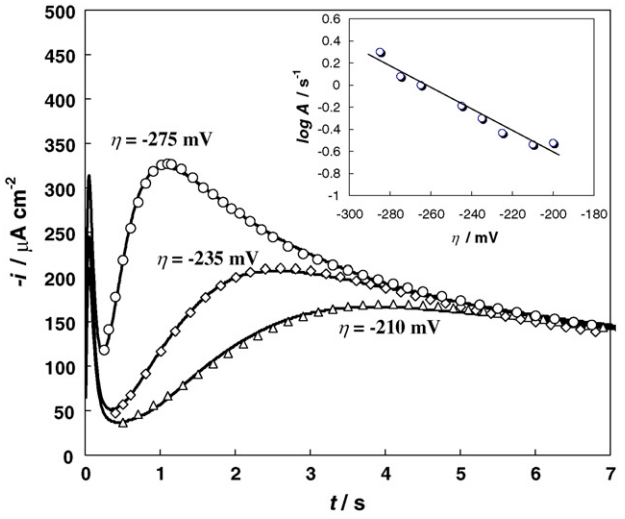

Fig. 4. Comparison between three experimental current transients recorded during Pd electrodeposition onto VC, and the corresponding theoretical current transients generated by non-linear fitting of Eq. (3) to the experimental data. The inset shows the overpotential dependence of the nucleation rate constant, *A*.

Table 2
Kinetic parameters extracted from the current transients for Pd nucleation on VC.

η (mV)	A (s^{-1})	N_0 ($\times 10^{-6}$ cm^{-2})	D ($\times 10^{6}$ $cm\,s^{-1}$)
−200	0.3	2.8	9.3
−210	0.29	4.2	8.9
−225	0.37	4.4	8.8
−235	0.50	4.7	8.8
−245	0.65	5.0	9.0
−265	1.0	8.7	9.0
−275	1.2	10.3	9.0
−285	2.0	16.0	8.8

tion on the surface with a larger fraction of sites becoming active as the cathodic overpotential is increased [24].

Considering the atomistic theory of nucleation [28,29], it is possible to express the nucleation rate constant *A* as:

$$A = k^{+} \exp\left[\frac{-\phi(n_k)}{kT}\right] \exp\left[\frac{(n_k - \beta)ze\eta}{kT}\right] \quad (6)$$

where β is the transition coefficient, ϕ (n_k) account for the nucleus–substrate interaction, k^{+} is the frequency factor and n_k the number of atoms in the critical nucleus. Therefore, n_k can be

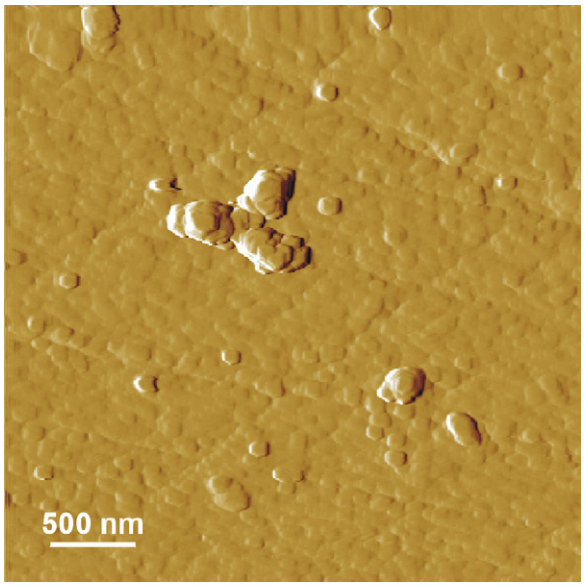

Fig. 6. AFM image of a Pd dendritic structure formed on the VC surface at $\eta = -285$ mV, $t_p = 20$ s.

obtained using:

$$n_k = \left(\frac{2.3023RT}{zF}\right)\left(\frac{d\ \log A}{d\eta}\right) \quad (7)$$

From the slope of the straight line in Fig. 4 and using Eq. (7) a value of $n_k \approx 0$ was obtained, and in terms of the atomistic theory of nucleation this means that a simple atom adsorbed on the surface forms a stable cluster that can grow irreversibly.

3.1.3. Morphological studies

Structural information of the palladium deposits formed on VC was obtained from ex situ atomic force microscopy (AFM) studies. At relatively low magnifications the VC surface appears smooth showing typical polishing lines, and nodule-like features, characteristics of this substrate [30], are observed at high magnifications. Fig. 5 shows ex situ AFM images of palladium crystals deposited on VC after stepping the potential from $E = 700$ mV to two different overpotential values. Both images of these Pd/VC modified surfaces show a distribution of palladium crystals sizes. The size of the Pd particles increases with time and the overpotential, consistent with the progressive nucleation mechanism. The deposits possess clear 3D characteristics with hemispherical morphology, appearing either randomly distributed or decorating the polishing lines or other surface defects indicating that these defects act as active

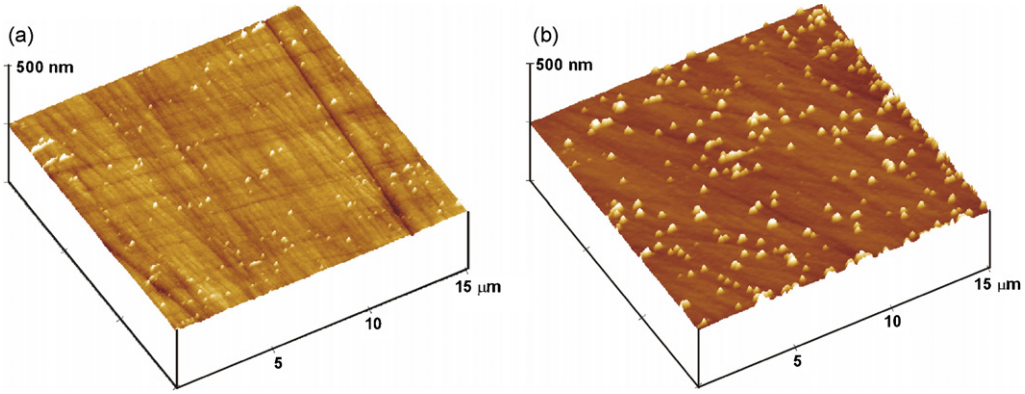

Fig. 5. AFM images of Pd deposits formed on the VC surface from the 9.5×10^{-4} M $PdCl_2$ + 0.1 M Na_2SO_4 + 2.4×10^{-2} M HCl solution at (a) $\eta = -200$ mV and (b) $\eta = -285$ mV. Polarization time, $t_p = 10$ s.

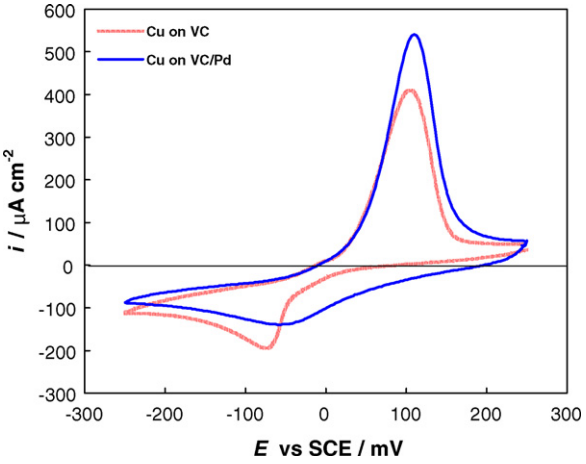

Fig. 7. Cyclic voltammogram obtained in 1×10^{-3} M $CuSO_4$ + 0.1 M Na_2SO_4 solution for a Pd/VC modified surface (Pd/VC obtained in 9.5×10^{-4} M $PdCl_2$ + 0.1 M Na_2SO_4 + 2.4×10^{-2} M HCl solution, $\eta = -285$ mV, $t_p = 10$ s). A cyclic voltammogram for bare VC surface in the same solution is also included for comparison purpose.

sites for the deposition. In some cases the palladium crystals grow on top of other previously deposited Pd particles forming dimers, trimers and chains of islands, and in some images the initial stages of dendritic growth are also observed (Fig. 6). The formation of dendritic structures was also informed during the electrodeposition of Pd onto highly oriented pyrolitic graphite (HOPG) [6].

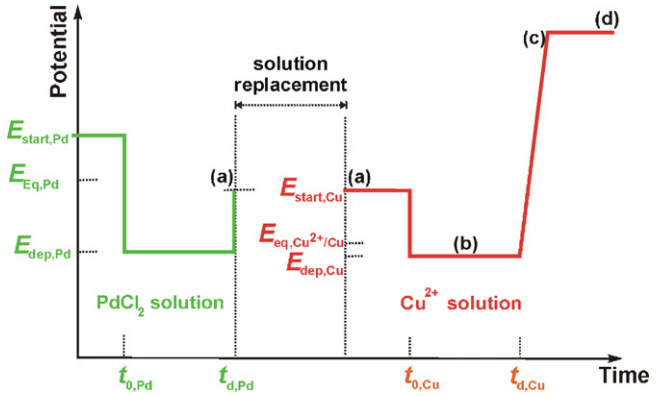

Fig. 8. Polarization routine applied to obtain Cu/Pd bimetallic crystals on vitreous carbon. The letters corresponds qualitatively to the potentials where the images of Fig. 9 were obtained.

3.2. Formation of Cu/Pd crystals

The formation of Cu/Pd bimetallic particles could be produced by sequential electrodeposition of both metals from 9.5×10^{-4} M $PdCl_2$ + 0.1 M Na_2SO_4 + 2.4×10^{-2} M HCl and 1×10^{-3} M $CuSO_4$ + 0.1 M Na_2SO_4 solutions, respectively. A similar method based on the "avalanche nucleation" phenomenon described by Deutscher and Fletcher [31] was applied by Penner et al. [32] to produce Ag/Cu core–shell bimetallic particles on HOPG.

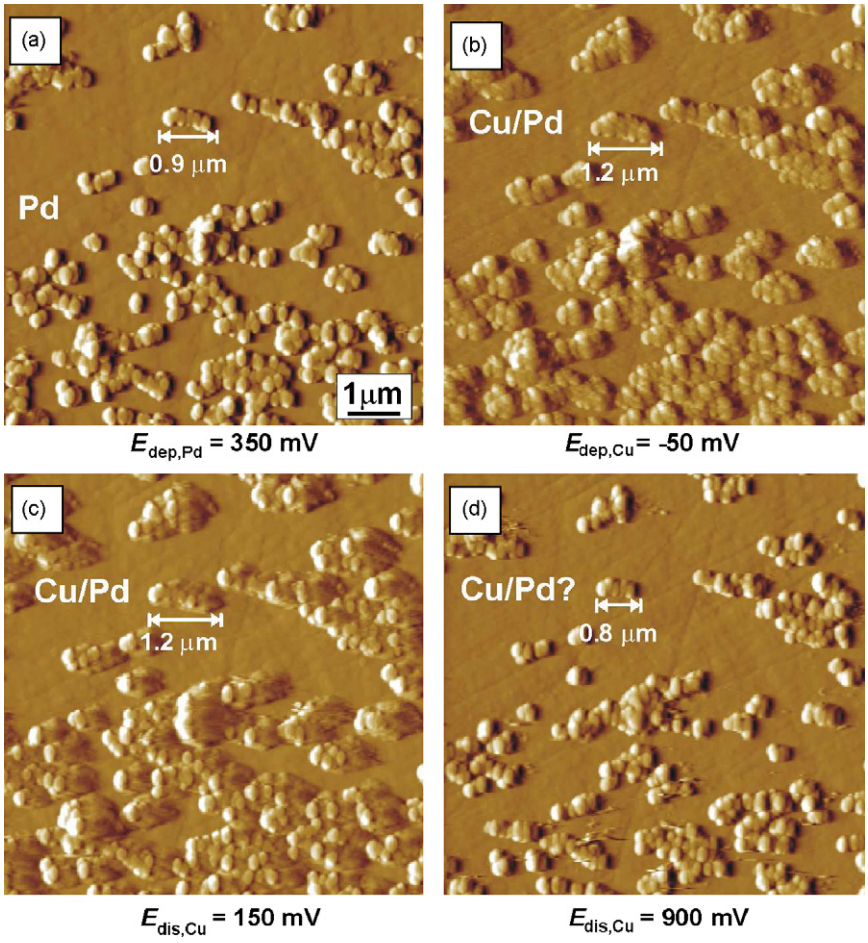

Fig. 9. Sequence of in situ AFM images obtained after the formation and subsequent dissolution of the Cu/Pd bimetallic crystals formed on VC according to the polarization routine shown in Fig. 8. (a) Pd crystals formed on VC; (b) formation of Cu/Pd core–shell structures; (c) and (d) anodic stripping of the Cu/Pd structures. Solutions: (a) 9.5×10^{-4} M $PdCl_2$ + 0.1 M Na_2SO_4 + 2.4×10^{-2} M HCl; (b)–(d) 1×10^{-3} M $CuSO_4$ + 0.1 M Na_2SO_4.

Therefore, and according to the experiments presented in previous paragraphs, the first step corresponds to the electrodeposition of Pd crystals on the VC surface from the Pd(II) containing solution. Afterwards, this Pd/VC modified surface would be polarized in the electrolyte containing only Cu^{2+} ions. Cu/Pd bimetallic particles could be formed if a selective electrodeposition of Cu onto the Pd crystallites takes place from this solution.

Fig. 7 shows the voltammetric behaviour of VC and a Pd/VC modified surface in the solution containing Cu^{2+} ions. It is clearly observed that the deposition of Cu on the Pd/VC modified surface initiates at potentials values more positive than that recorded with the clean VC surface. This effect could be related to the underpotential deposition (*upd*) process of Cu onto the Pd crystallites. The *upd* process is well know in this system [33] and, therefore, it is expected a high interaction energy between both metals that will enhance the selectivity for the deposition of Cu onto the Pd particles.

Considering the voltammetric curves shown in Figs. 1 and 7, the polarization routine used to prepare Cu/Pd bimetallic particles is schematized in Fig. 8. This polarization routine was applied directly in the AFM cell in order to follow the morphological changes during the experiment. Initially, Pd particles were deposited onto the VC surface from the Pd(II) containing solution, applying a potential step from $E_{start} = 700$ mV to $E_{dep,Pd} = 115$ mV ($\eta_{Pd} = -285$ mV) during $t = 10$ s. Afterwards, the potential was fixed at $E = 350$ mV ($\eta_{Pd} = -50$ mV) in order to obtain the initial AFM image of the Pd particles, shown in Fig. 9a. Subsequently, the imaging process was stopped and the electrolyte of the AFM fluid cell was gently removed and changed, initially by fourfold quartz-distilled water, and then by 1×10^{-3} M $CuSO_4$ + 0.1 M Na_2SO_4 (pH 2.6) solution. All these operations required great care so as to not change the surface location imaged by the AFM tip. After the introduction of the Cu^{2+} electrolyte the potential was immediately fixed at $E_{start,Cu} = 350$ mV and the surface imaged again verifying that the place and the Pd crystals were not changed during the operations described above. Afterwards, the electrode potential was changed to $E_{dep,Cu} = -50$ mV producing the Cu deposition. As it is shown in Fig. 9b, the Cu deposition occurs selectively forming a core–shell structure with a thin layer of Cu covering the Pd crystals. Finally, this Cu/Pd/VC modified surface was polarized at more positive potentials (Fig. 9c) in order to produce the anodic stripping of the Cu deposit. It is interesting to note that very positive potentials relative to the Cu^{2+}/Cu^0 equilibrium potential ($E_{eq,Cu^{2+}/Cu^0} = 10$ mV) were necessary to produce the total stripping of the Cu (Fig. 9d). This behaviour could be explained considering the formation of a Cu–Pd alloy by mutual interdiffusion to the Pd and Cu atoms. This alloying process would stabilize the bimetallic crystallites and, therefore, a relatively high overpotential is required to produce its dissolution. A similar behaviour was also observed during the stripping of Ag–Cd surface alloys phases [34,35]. The reproducibility of the previous experiment was studied polarizing the VC electrode in conventional electrochemical cells following the polarization routine previously described. After that, scanning electron microscopy (SEM) images and the corresponding EDX analysis obtained on different places of the VC surface, also evidenced the selective electrodeposition of Cu onto the Pd crystallites (Fig. 10), leading the formation of Cu/Pd bimetallic structures.

Finally, Fig. 11 shows the anodic stripping curve (a) of the Cu/Pd/VC modified surface performed in 0.1 M Na_2SO_4 (pH 2.6) solution using a conventional electrochemical cell. This modified surface was prepared polarizing the Pd/VC surface at $E_{dep,Cu} = -50$ mV in the Cu^{2+} containing solution during a polarizing time $t_p = 500$ s. The anodic stripping produces the peak A_1 related to the dissolution of Cu followed by another one, A_2, related to the oxidation of the Pd particles. Fig. 11 also shows the anodic polarization curve (b) of a VC surface, free of Pd deposits, previously polarized

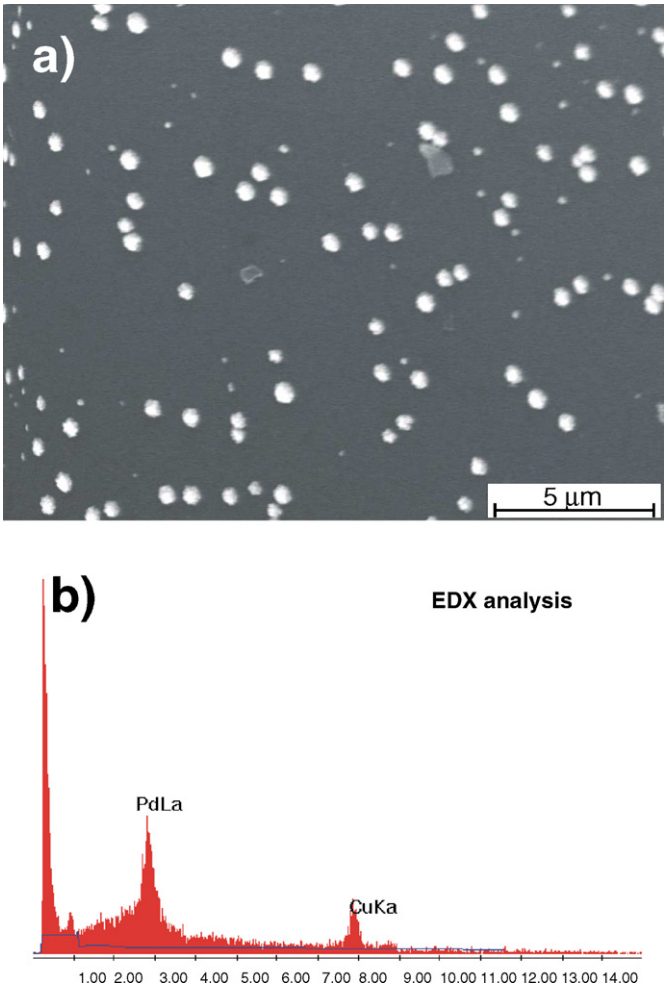

Fig. 10. (a) SEM image obtained on the Cu/Pd/VC modified surface showing the presence of microcrystallites; (b) the corresponding EDX analysis performed on one of the crystallites indicating the selective electrodeposition of Cu on Pd.

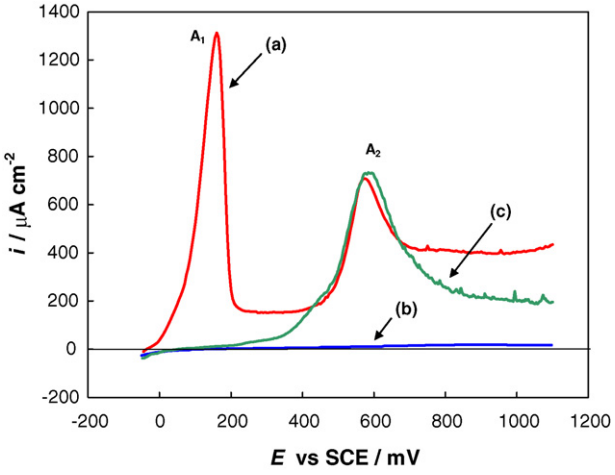

Fig. 11. Anodic polarization curves obtained in 0.1 M Na_2SO_4 (pH 2.6) solution for (a) Pd/VC surface ( ) and (b) VC substrate ( ), both previously polarized at $E = -50$ mV during $t_p = 500$ s in the Cu^{2+} solution; (c) Pd/VC modified substrate without any pretreatment ( ). $|dE/dt| = 10$ mV s^{-1}. (For interpretation of the references to color in this figure legend, the reader is referred to the web version of the article.)

at $E = -50$ mV in the Cu^{2+} containing solution also during $t_p = 500$ s. In this case no anodic peak related to the Cu dissolution is observed which prove that, at the potential considered, the copper deposition is favoured by the presence of Pd onto the substrate surface. In addition, in Fig. 11 was also included the anodic polarization curve (c) corresponding to the Pd/VC surface in order to verify that the anodic peak A_2 is associated with the oxidation of the Pd particles. It is important to mention that the Cu stripping charge recorded from the Cu/Pd/VC substrate was quite lower than that related to the Cu deposition charge recorded during t_p. This fact is further evidence for the formation of a Cu–Pd alloy and is in agreement with the AFM images.

4. Conclusions

In this work the very initial stages of the palladium electrodeposition process on vitreous carbon from a 9.5×10^{-4} M $PdCl_2$ + 0.1 M Na_2SO_4 + 2.4×10^{-2} M HCl solution were analysed. Within the potential range considered the kinetics of the Pd electrodeposition can be described by a model involving progressive nucleation on active sites and diffusion-controlled 3D growth. The nucleation rate constant, A_0, and the number of active sites of the substrate, N_0, were determined from the analysis of potentiostatic current transients on the basis of the Hermann and Tarallo theoretical model. The AFM images corroborated the progressive nucleation mechanism showing irregular palladium crystals randomly distributed over the VC surface, with different sizes and 3D morphological characteristics. The electrodeposition of Cu was carried out onto the characterized Pd/VC modified surface from a Cu^{2+} containing solution using a well defined polarization routine. The SEM/EDX images confirmed the formation of Cu/Pd bimetallic crystals uniformly distributed on the VC surface and the in situ AFM images obtained during this process corroborated that Cu formed a core–shell structure with the Pd crystals. Nevertheless, the subsequent anodic stripping produced only a partial dissolution of the Cu deposits, and therefore, the formation of a Cu–Pd alloy could be inferred. The electrochemical method described to obtain the Cu/Pd bimetallic system is an extension of that described by Penner et al. [32] and could be considered as an alternative to prepare other bimetallic systems on VC such as those used as catalyst in fuel cells and other technological systems.

Acknowledgements

The authors wish to thank the Universidad Nacional del Sur, Argentina, and the Agencia de Promoción Científica (PICTO-UNS 2004 Cod. 614) for financial support of this work.

References

[1] V.S. Bagotsky, "Fundamentals of Electrochemistry (second edition)". Chapter 28: Electrocatalysis, John Wiley & Sons, Inc., 2006, p. 521.
[2] E. Budevski, G. Staikov, W.J. Lorenz, Electrochemical Phase Formation and Growth, VCH, 1996.
[3] J. Tsuji, Palladium Reagents and Catalysts, Wiley, Chichester, UK, 1996.
[4] R.S. Jayashree, J.S. Spendelow, J. Yeom, C. Rastogi, M.A. Shannon, P.J.A. Kenis, Electrochim. Acta 50 (2005) 4674.
[5] F. Li, B. Zhang, S. Dong, E. Wang, Electrochim. Acta 42 (1997) 2563.
[6] Y. Gimeno, A. Hernández Creus, P. Carro, S. González, R.C. Salvarezza, A.J. Arvia, J. Phys. Chem. B 106 (2002) 4232.
[7] C.G. Sanchez, E.P.M. Leiva, W. Schmickler, Electrochem. Commun. 5 (2003) 584.
[8] D. Bera, S.C. Kuiry, S. Seal, J. Phys. Chem. B 108 (2004) 556.
[9] A.C.A. de Vooys, R.A. van Santen, J.A.R. van Veen, J. Mol. Catal. A: Chem. 154 (2000) 203.
[10] M. Ilieva, V. Tsakova, W. Erfurth, Electrochim. Acta 52 (2006) 816.
[11] L. Szpyrkowicz, S. Daniele, M. Radaelli, S. Specchia, Appl. Catal. B: Environ. 66 (2006) 40.
[12] S.N. Pronkin, P.A. Simonov, V.I. Zaikovskii, E.R. Savinova, J. Mol. Catal. A: Chem. 265 (2007) p141.
[13] C. Milano, D. Pletcher, J. Electroanal. Chem. 614 (2008) 24.
[14] A. Franco, S. Passot, P. Fugier, C. Anglade, E. Billy, L. Guétaz, N. Guillet, E. De Vito, S. Mailley, J. Electrochem. Soc. 156 (2009) pB410.
[15] A. Franco, S. Passot, P. Fugier, C. Anglade, E. Billy, L. Guétaz, N. Guillet, E. De Vito, S. Mailley, ECS Trans. 13 (2008) 29.
[16] A. Züttel, Ch. Nützenadel, G. Schmid, Ch. Emmenegger, P. Sudan, L. Schlapbach, Appl. Surf. Sci. 571 (2000) 162.
[17] P. Millet, M. Srour, R. Faure, R. Durand, Electrochem. Commun. 3 (2001) 478.
[18] S. Fletcher, C.S. Halliday, D. Gates, M. Westcott, T. Lwin, G. Nelson, J. Electroanal. Chem. 159 (1983) 267.
[19] R.M. Smith, A.R. Martell, Critical Stability Constants, vol. 4, Plenum Press, 1976.
[20] A.J. Bard, R. Parsons, J. Jordan (Eds.), Standard Potential in Aqueous Solutions, IUPAC and Marcel Dekker, 1985.
[21] B. Scharifker, G. Hills, Electrochim. Acta 28 (1983) 879.
[22] B.R. Scharifker, J. Mostany, J. Electroanal. Chem. 177 (1984) 13.
[23] M. Sluyters-Rehbach, J.H.O.J. Wijenber, E. Bosco, J.H. Sluyters, J. Electroanal. Chem. 236 (1987) 1.
[24] R.L. Deutscher, S. Fletcher, J. Electroanal. Chem. 239 (1988) 17.
[25] A. Milchev, J. Electroanal. Chem. 457 (1998) 35.
[26] L. Heerman, A. Tarallo, J. Electroanal. Chem. 470 (1999) 70.
[27] M.E. Hyde, R.G. Compton, J. Electroanal. Chem. 549 (2003) 1.
[28] A. Milchev, S. Stoyanov, R. Kaischev, Thin Solid Films 22 (1974) 255.
[29] A. Milchev, S. Stoyanov, J. Electroanal. Chem. 72 (1976) 33.
[30] M. Miranda-Hernández, M. Palomar-Pardavé, N. Batina, I.J. González, J. Electroanal. Chem. 443 (1998) 81.
[31] R.L. Deutscher, S. Fletcher, J. Electroanal. Chem. 277 (1990) 1.
[32] H. Kwok, Rg.N.M. Penner, J. Electroanal. Chem. 522 (2002) 86.
[33] T. Chierchie, C. Mayer, Electrochim. Acta 33 (1988) 341.
[34] S.G. García, D.R. Salinas, G. Staikov, Surf. Sci. 576 (2005) 9.
[35] M.C. del Barrio, S.G. García, D.R. Salinas, Electrochem. Commun. 6 (2004) 762.